

# ELUCIDATING $\Lambda$ CDM: IMPACT OF BARYON ACOUSTIC OSCILLATION MEASUREMENTS ON THE HUBBLE CONSTANT DISCREPANCY

G. E. ADDISON<sup>1</sup>, D. J. WATTS<sup>1</sup>, C. L. BENNETT<sup>1</sup>, M. HALPERN<sup>2</sup>, G. HINSHAW<sup>2</sup>, AND J. L. WEILAND<sup>1</sup>

*Draft version February 1, 2018*

## ABSTRACT

We examine the impact of baryon acoustic oscillation (BAO) scale measurements on the discrepancy between the value of the Hubble constant ( $H_0$ ) inferred from the local distance ladder and from *Planck* cosmic microwave background (CMB) data. While the BAO data alone cannot constrain  $H_0$ , we show that combining the latest BAO results with *WMAP*, Atacama Cosmology Telescope (ACT), or South Pole Telescope (SPT) CMB data produces values of  $H_0$  that are  $2.4 - 3.1\sigma$  lower than the distance ladder, independent of *Planck*, and that this downward pull was less apparent in some earlier analyses that used only angle-averaged BAO scale constraints rather than full anisotropic information. At the same time, the combination of BAO and CMB data also disfavors the lower values of  $H_0$  preferred by the *Planck* high-multipole temperature power spectrum. Combining galaxy and Lyman- $\alpha$  forest (Ly $\alpha$ ) BAO with a precise estimate of the primordial deuterium abundance produces  $H_0 = 66.98 \pm 1.18 \text{ km s}^{-1} \text{ Mpc}^{-1}$  for the flat  $\Lambda$ CDM model. This value is completely independent of CMB anisotropy constraints and is  $3.0\sigma$  lower than the latest distance ladder constraint, although  $2.4\sigma$  tension also exists between the galaxy BAO and Ly $\alpha$  BAO. These results show that it is not possible to explain the  $H_0$  disagreement solely with a systematic error specific to the *Planck* data. The fact that tensions remain even after the removal of any single data set makes this intriguing puzzle all the more challenging to resolve.

*Keywords:* cosmic background radiation – cosmological parameters – cosmology: observations – distance scale – large-scale structure of universe

## 1. INTRODUCTION

While no single data set currently provides compelling evidence for a deviation from the standard Lambda cold dark matter ( $\Lambda$ CDM) cosmological model, the values of some parameters inferred from different measurements now exhibit moderate to severe tension. This is most pronounced in the value of the Hubble constant,  $H_0$ . Riess et al. (2016; hereafter R16) provided the most recent and most precise local distance ladder constraint, finding  $H_0 = 73.24 \pm 1.74 \text{ km s}^{-1} \text{ Mpc}^{-1}$  by combining three absolute distance anchors with the empirical period-luminosity relation for Cepheid variable stars and the relationship between observed light curve and intrinsic luminosity of type Ia supernovae (SNe). The most precise  $H_0$  prediction from cosmic microwave background (CMB) anisotropy power spectrum measurements is currently provided by the *Planck* mission. The 2015 *Planck* temperature and polarization analysis produced  $H_0 = 67.31 \pm 0.96 \text{ km s}^{-1} \text{ Mpc}^{-1}$  (Planck Collaboration et al. 2016). An updated analysis with a revised estimate of the optical depth to reionization,  $\tau$ , found  $H_0 = 66.88 \pm 0.91$ , or  $66.93 \pm 0.62$  if preliminary small-scale polarization data are also included (Planck Collaboration Int. XLVI 2016). Assuming all uncertainties are Gaussian, these values are, respectively,  $3.0$ ,  $3.2$ , and  $3.4\sigma$  lower than the distance ladder determination. Strong lensing timing delay measurements have produced  $H_0$  constraints consis-

tent with the distance ladder, and in mild tension with *Planck* (Bonvin et al. 2017). Tensions also exist between the *Planck* predictions for the growth of cosmic structure (through the matter density,  $\Omega_m$ , and present-day density fluctuation amplitude,  $\sigma_8$ ) and measurements using weak gravitational lensing (e.g., Hildebrandt et al. 2017; Joudaki et al. 2017; Alsing et al. 2017; Köhlinger et al. 2017).

It is not clear whether the problem is with the model or the data. While it is certainly plausible that a failure of the standard model could show up as a discrepancy between the CMB and low-redshift measurements, none of the commonly-considered or physically-motivated extensions to  $\Lambda$ CDM appear to provide a convincing improvement when considering the full range of data available (e.g., Planck Collaboration et al. 2016; Bernal et al. 2016). In principle, the CMB prediction for  $H_0$  could be significantly increased by modifying the expansion history of the universe post-recombination, for example by allowing spatial curvature or a dark energy equation of state  $w \neq -1$ . *Planck* temperature and polarization data alone mildly prefer a non-zero curvature, but  $H_0$  goes in the wrong direction. The *Planck* 2015  $\Lambda$ CDM+ $\Omega_k$  constraint is  $53.2 \pm 5.1 \text{ km s}^{-1} \text{ Mpc}^{-1}$  (mean and standard deviation), with 95% of Markov chain Monte Carlo (MCMC) samples lying in  $43.7 < H_0 / \text{km s}^{-1} \text{ Mpc}^{-1} < 63.5^3$ . Allowing  $w < -1$  can shift the *Planck* prediction to 70 or even  $80 \text{ km s}^{-1} \text{ Mpc}^{-1}$ , however, even leaving aside questions of the physical interpretation of  $w < -1$ , resolving the  $H_0$  disagreement with evolution in  $w$  is strongly disfavored when we include ob-

gaddison@jhu.edu

<sup>1</sup> Dept. of Physics & Astronomy, The Johns Hopkins University, 3400 N. Charles St., Baltimore, MD 21218-2686

<sup>2</sup> Department of Physics and Astronomy, University of British Columbia, 6224 Agricultural Road, Vancouver, BC V6T 1Z1, Canada

<sup>3</sup> The public *Planck* MCMC chains can be downloaded from the *Planck* legacy archive: <http://pla.esac.esa.int/pla/>

servations of the expansion rate, such as baryon acoustic oscillations (BAO) in the clustering of galaxies, or high-redshift SNe. Alam et al. (2017) combined *Planck* data with the latest galaxy clustering and SNe data and found  $H_0 = 67.9 \pm 0.9 \text{ km s}^{-1} \text{ Mpc}^{-1}$  for constant  $w$ , or  $67.5 \pm 1.0 \text{ km s}^{-1} \text{ Mpc}^{-1}$  for the  $w_0 - w_a$  parameterization.

Modifying the early-universe expansion history, for instance by increasing the number of effective neutrino species,  $N_{\text{eff}}$ , can increase the CMB  $H_0$  prediction. The *Planck* data do not favor this solution, for example Alam et al. (2017) report  $N_{\text{eff}} = 2.97 \pm 0.20$  (*Planck*-only), and  $3.03 \pm 0.18$  (*Planck* plus galaxy clustering), consistent with the standard model value of 3.046, with corresponding  $H_0$  constraints of  $66.6 \pm 1.6$  and  $67.5 \pm 1.2 \text{ km s}^{-1} \text{ Mpc}^{-1}$ . Adding  $N_{\text{eff}}$  in these fits shifted the tension with the distance ladder from  $3.2\sigma$  to  $2.8\sigma$  (*Planck*-only) and from  $3.1\sigma$  to  $2.7\sigma$  (*Planck* plus galaxy clustering). A fit to the 2015 *Planck* temperature and polarization data plus BAO fixing  $N_{\text{eff}} = 3.4$ , the value found by R16 to most effectively relieve *Planck*-distance ladder tension, leads to an increase in the parameter combination best constrained by weak lensing measurements,  $\sigma_8 \Omega_m^{0.5}$ , by around 1.5%, 0.8 times the original uncertainty<sup>4</sup>. This slightly worsens the tension between *Planck* and the weak lensing analyses mentioned above, which found  $\sigma_8 \Omega_m^{0.5}$  values lower than *Planck* at the  $2-3\sigma$  level when the standard model was assumed. Brust et al. (2017) found that the *Planck*-lensing consistency could be improved by also introducing some degree of neutrino or dark radiation self-interaction, but, even with a second additional parameter, a joint fit to the *Planck*, BAO, distance ladder, weak lensing, and galaxy cluster data produced a  $H_0$  distribution peaking at  $69.95 \text{ km s}^{-1} \text{ Mpc}^{-1}$ , still almost  $2\sigma$  lower than the R16 measurement. In short, while a non-standard value of  $N_{\text{eff}}$  cannot be ruled out, its inclusion is not justified by the improvements to the fit.

On the other hand, the discrepant data sets have passed a range of systematic checks. The R16 distance ladder analysis used infrared data to greatly reduce the effects of reddening, substituted rungs of the ladder with alternative data, compared different calibrators, corrected for estimated local motion, and constructed a systematic error budget from considering a range of modeling variants (see also, e.g., Cardona et al. 2017; Zhang et al. 2017; Feeney et al. 2017; Dhawan et al. 2017; Follin & Knox 2017). The distance ladder measurements have substantially improved since the analysis by Efstathiou (2014). While the constraints have become tighter, the mean  $H_0$  values in recent years have remained fairly constant (e.g., Riess et al. 2009, 2011; Freedman et al. 2012). Likewise, the *Planck* team has performed an array of robustness checks of their data, investigating the effects of detector nonlinearity, beam shapes and sidelobes, and various other calibration-related issues. Also, the preference for a lower  $H_0$  from *Planck* does not appear to be driven by a particular frequency channel (Planck Collaboration Int. LI 2016).

Ultimately it may take additional high-precision mea-

surements to shed light on what is really going on. More precise measurements may bring with them new tensions or disagreements, and the handling of systematic errors will get harder, not easier, as statistical uncertainties are reduced. In the meantime, it is therefore helpful to re-examine existing data and ask whether any extra insight into the discrepancies can be gleaned. To this end, in this paper we investigate in detail the indirect but important role played by BAO measurements in  $H_0$  constraints, both with and without CMB anisotropy data. While this topic has been addressed in the literature, we describe several results that have either not previously been discussed, or are not widely appreciated. In Section 2, we review the BAO measurements. In Section 3, we describe results of fitting cosmological parameters to BAO in conjunction with other data sets, focussing on  $H_0$ . A discussion and conclusions follow in Sections 4 and 5.

## 2. BAO MEASUREMENTS

The first convincing detections of the BAO feature in the correlation function or power spectrum of large-scale structure (LSS) tracers were made a little over a decade ago (Eisenstein et al. 2005; Cole et al. 2005). Since that time, deeper surveys with orders of magnitude more galaxies, notably the Baryon Oscillation Spectroscopic Survey (BOSS<sup>5</sup>), have led to both improved precision in the BAO scale measurements over a range of redshifts, and improved analysis methodologies (e.g., Percival et al. 2014; Anderson et al. 2014; Kazin et al. 2014; Reid et al. 2016). While current and future BAO surveys are proposed as a means of improving dark energy constraints, BAO measurements also provide significant information about parameters in the standard  $\Lambda$ CDM model, particularly in joint fits with the CMB.

A detailed discussion of BAO physics can be found in Chapter 4 of Weinberg et al. (2013). The BAO scale in the transverse and line-of-sight direction correspond to measurements of  $D_M(z)/r_d$  and  $H(z)r_d$ , where  $D_M(z) = (1+z)D_A(z)$  is the comoving angular diameter distance at the effective redshift of the survey and  $r_d$  is the sound horizon at the drag epoch where baryons decouple from photons, denoted  $z_d$ . The sound horizon is defined as<sup>6</sup>

$$r_d = \int_{z_d}^{\infty} dz \frac{c_s(z)}{H(z)}, \quad (1)$$

where the sound speed,  $c_s = c/\sqrt{3(1+R)}$ , depends on the ratio of baryon to photon density, with  $R = 3\rho_b/4\rho_\gamma$ . The sound horizon is sensitive to the physics of the early universe, including the pre-recombination expansion history and the number of effective neutrino species,  $N_{\text{eff}}$ , while  $D_M(z)$  and  $H(z)$  at the effective redshift of the survey depend on the late-time expansion.

In some cases, only a joint constraint, for example on  $D_V(z)/r_d$ , where  $D_V(z) = [czD_M^2(z)/H(z)]^{1/3}$ , is provided, representing an angle-averaged constraint. This can be helpful where the BAO feature is detected at lower significance and the separate line-of-sight and transverse

<sup>5</sup> <http://www.sdss3.org/surveys/boss.php>

<sup>6</sup> The sound horizon was referred to as  $r_s$  by Addison et al. (2013), we have adopted the  $r_d$  notation here for consistency with other work.

<sup>4</sup> This result is taken from the *Planck* 2015 base\_plikHM\_TTTEEE\_lowTEB\_post\_BAO and base\_nnu\_plikHM\_TTTEEE\_lowTEB\_nnup39\_BAO chains.

**Table 1**  
BAO measurements used in this work

Dataset	LSS tracer	$z_{\text{eff}}$	Measurement <sup>a</sup>	Constraint <sup>a</sup>	Reference
6dFGS	galaxies	0.106	$r_d/D_V(z_{\text{eff}})$	$0.336 \pm 0.015$	Beutler et al. (2011)
SDSS MGS	galaxies	0.15	$D_V(z_{\text{eff}}) r_{d,\text{fid.}}/r_d$ [Mpc]	$664 \pm 25$	Ross et al. (2015)
BOSS DR12	galaxies	0.38	$D_M(z_{\text{eff}}) r_d/r_{d,\text{fid.}}$ [Mpc]	$1512 \pm 25$	Alam et al. (2017)
			$H(z_{\text{eff}}) r_d/r_{d,\text{fid.}}$ [km s <sup>-1</sup> Mpc <sup>-1</sup> ]	$81.2 \pm 2.4$	
		0.51	$D_M(z_{\text{eff}}) r_d/r_{d,\text{fid.}}$ [Mpc]	$1975 \pm 30$	
			$H(z_{\text{eff}}) r_d/r_{d,\text{fid.}}$ [km s <sup>-1</sup> Mpc <sup>-1</sup> ]	$90.9 \pm 2.3$	
		0.61	$D_M(z_{\text{eff}}) r_d/r_{d,\text{fid.}}$ [Mpc]	$2307 \pm 37$	
			$H(z_{\text{eff}}) r_d/r_{d,\text{fid.}}$ [km s <sup>-1</sup> Mpc <sup>-1</sup> ]	$99.0 \pm 2.5$	
BOSS DR11 Ly $\alpha$	Ly $\alpha$ absorbers <sup>b</sup>	2.34	$D_A(z_{\text{eff}})/r_d$ $c/[H(z_{\text{eff}})r_d]$	$11.28 \pm 0.65$ $9.18 \pm 0.28$	Delubac et al. (2015)
BOSS DR11 QSO $\times$ Ly $\alpha$	QSO, Ly $\alpha$ <sup>b</sup>	2.36	$D_A(z_{\text{eff}})/r_d$ $c/[H(z_{\text{eff}})r_d]$	$10.8 \pm 0.4$ $9.0 \pm 0.3$	Font-Ribera et al. (2014)

<sup>a</sup>Note that the fiducial sound horizon,  $r_{d,\text{fid.}}$ , differs across different analyses. We provide constraints here only to show relative precision. For parameter fitting we use full likelihood surfaces, including correlations across the BOSS redshift bins or between  $D_M$  and  $H$ .

<sup>b</sup>For brevity we refer to the Ly $\alpha$  and QSO $\times$ Ly $\alpha$  measurements collectively as Ly $\alpha$ .

measures are poorly constrained or have distributions with non-Gaussian tails. Whenever possible, we use the joint anisotropic  $D_M(z)/r_d$  and  $H(z)r_d$  constraints. Quantities like  $D_V(z)/r_d$  entail a compression of information that potentially give a false sense of agreement with other data, as discussed in Section 3.2.

### 2.1. Current BAO constraints

The BAO data sets included in fits presented in this paper are listed in Table 1. For the 6dF Galaxy Survey (6dFGS) and Sloan Digital Sky Survey (SDSS) Main Galaxy Sample (MGS), we adopt a simple Gaussian likelihood for  $r_d/D_V(z)$  or  $D_V(z)/r_d$ . Away from the peak of the likelihood these constraints become non-Gaussian, however the uncertainties for these measurements are large enough that the preferred model solutions never lie far from the peak in a joint fit with other data. We use the consensus BAO scale measurements from the BOSS Data Release 12 (DR12), including  $D_M(z)/r_d$  and  $H(z)r_d$  for each of the three redshift bins and the six-by-six covariance matrix described by Alam et al. (2017). We restrict our analysis to the BAO scale as it is the most robust observable from LSS surveys (e.g., Weinberg et al. 2013, and references therein), and do not consider redshift-space distortion constraints or information from the broadband correlation function. We do not include results from the WiggleZ<sup>7</sup> survey, which are consistent with BOSS and partially overlap in sky coverage (Beutler et al. 2016).

BAO have been measured in the Lyman- $\alpha$  (Ly $\alpha$ ) forest of BOSS quasars (QSOs), and in the cross-correlation between the QSOs and Ly $\alpha$  absorbers, at effective redshifts of 2.3 – 2.4 (Busca et al. 2013; Slosar et al. 2013; Font-Ribera et al. 2014; Delubac et al. 2015; Bautista et al. 2017). BAO measurements at these redshifts, when the dark energy contribution to the total energy budget of the universe is small, are a powerful complement to the BAO from lower-redshift galaxy surveys. The analysis methodology and systematic error treatment required

to extract the Ly $\alpha$  BAO scale are less mature than for the galaxy BAO and are an active field of research (e.g., Blomqvist et al. 2015). The anisotropic BAO measurements from the DR11 Ly $\alpha$  and QSO $\times$ Ly $\alpha$  analyses are in  $\sim 2.5\sigma$  tension with *Planck* predictions assuming a standard flat  $\Lambda$ CDM model. This tension was reduced slightly in the DR12 Ly $\alpha$  BAO analysis (Bautista et al. 2017). Bautista et al. (2017) found that the shift in the DR12 Ly $\alpha$  constraints was predominantly due to the additional data rather than some different treatment of systematic effects<sup>8</sup>. We present results using the DR11 Ly $\alpha$  and QSO $\times$ Ly $\alpha$  constraints, and from combining the galaxy and Ly $\alpha$  BAO, noting that  $\sim 2.5\sigma$  effects can and do arise purely from statistical fluctuations, and that there is currently no known systematic error that explains this tension.

Other BAO measurements have been reported, for example using galaxy clusters as LSS tracers (e.g., Veropalumbo et al. 2016; Hong et al. 2016). These results are generally less precise than the galaxy BAO, at similar redshifts, and their inclusion would not significantly affect our results. Recently, the first measurement of BAO from the extended Baryon Oscillation Spectroscopic Survey (eBOSS<sup>9</sup>) was reported using clustering of quasars at  $0.8 \leq z \leq 2.2$  (Ata et al. 2017). BAO constraints from this redshift range are potentially a useful addition to the galaxy and Ly $\alpha$  BAO and upcoming, higher-precision eBOSS measurements will be interesting to include in future analyses.

### 2.2. Choice of CMB data for joint fits

Joint fits between *Planck* and BAO have been reported extensively for a range of cosmological models in recent work (e.g., Aubourg et al. 2015; *Planck* Collaboration et al. 2016; Alam et al. 2017). While *Planck* provides the most precise CMB constraints,  $\sim 2.5\sigma$  tension exists

<sup>8</sup> The DR12 QSO $\times$ Ly $\alpha$  analysis, released while this work was in review, produced results consistent with DR11, in tension with *Planck* predictions at the  $2.3\sigma$  level (du Mas des Bourboux et al. 2017)

<sup>9</sup> <http://www.sdss.org/surveys/eboss/>

<sup>7</sup> <http://wigglez.swin.edu.au/site/>

between determination of some parameters from splitting the *Planck* power spectrum into multipoles  $\ell < 800$  and  $\ell > 800$ , where the choice of 800 corresponds to a roughly even division of overall constraining power (Addison et al. 2016). In the full  $\Lambda$ CDM model space, the tension is not significant ( $1.8\sigma$  for the assumptions used by Addison et al. 2016; see also Planck Collaboration Int. LI 2016). Current low-redshift cosmological observations do not provide strong constraints across the full  $\Lambda$ CDM parameter space, however they do provide independent and precise constraints on a subset of parameters, including  $H_0$ ,  $\Omega_m$ , and  $\sigma_8$ . These parameters are therefore of particular interest when it comes to assessing the performance of the  $\Lambda$ CDM model and testing for alternatives. Given the moderate internal *Planck* tension in these parameters, it is informative to consider other CMB measurements to help understand the extent to which conclusions are driven by *Planck* data, or are independent of *Planck*. In this work we therefore also include results from the final WMAP 9-year analysis (Bennett et al. 2013; Hinshaw et al. 2013), the Atacama Cosmology Telescope polarization-sensitive receiver (ACT-Pol; Thornton et al. 2016; Louis et al. 2017; Sherwin et al. 2016) two-season survey, covering  $548 \text{ deg}^2$ , and the 2500  $\text{deg}^2$  South Pole Telescope Sunyaev-Zel’dovich survey (SPT-SZ; Carlstrom et al. 2011; Story et al. 2013; van Engelen et al. 2012).

### 3. RESULTS

#### 3.1. Combining BAO and CMB anisotropy measurements

In Table 2 we show  $H_0$  constraints within the  $\Lambda$ CDM model from CMB data sets with and without the inclusion of the BAO data. ACTPol and SPT use WMAP or *Planck* data only to provide an absolute calibration, that is, a single scale-independent multiplicative rescaling of the measured power spectrum. Since these experiments do not measure  $\tau$ , we adopt a Gaussian prior, either the same broader  $\tau = 0.07 \pm 0.02$  prior used by Planck Collaboration XI (2016) and Addison et al. (2016), or the  $\tau = 0.055 \pm 0.009$  constraint from the latest *Planck* HFI low- $\ell$  polarization determination (Planck Collaboration Int. XLVI 2016). Here and throughout this paper we quote the mean and standard deviation from MCMC runs using the `CosmoMC`<sup>10</sup> package (Lewis & Bridle 2002), with convergence criterion  $R - 1 < 0.01$  (Gelman & Rubin 1992). Since we are not investigating foreground modeling in this work we use foreground-marginalized CMB likelihood codes for ACTPol and SPT (Dunkley et al. 2013; Calabrese et al. 2013). Uncertainties in foreground and other nuisance parameters propagate to cosmological parameters through an increase in power spectrum uncertainties in these codes. In the *Planck* rows of Table 2 we include the exact name of the likelihood file for clarity since a range of likelihoods have been provided by the *Planck* collaboration. These likelihoods include *Planck* foreground and nuisance parameters as described by Planck Collaboration XI (2016). We show results with and without CMB lensing power spectra (denoted ‘ $\phi\phi$ ’ in the third column of Table 2), noting that the lensing measurements have a moderate effect on

some of the CMB-only constraints but reduced impact when the BAO are included. In the last four rows of Table 2 we also list constraints from splitting the *Planck* temperature power spectrum at  $\ell = 800$  (Addison et al. 2016), as mentioned in Section 2.2 and discussed further in Section 4.

Adding galaxy BAO to any of the CMB measurements listed in Table 2 substantially tightens the  $H_0$  prediction, by more than a factor of three in the case of ACTPol or SPT. While there is still scatter in the CMB + galaxy BAO  $H_0$  values, the spread is substantially reduced compared to the CMB-only column. The ACTPol+BAO and SPT+BAO combinations produce  $H_0$  constraints of comparable precision to *Planck* alone. The synergy between the galaxy BAO and CMB measurements for  $\Lambda$ CDM is illustrated in Figure 1 using the BOSS DR12 anisotropic BAO measurements at  $z_{\text{eff}} = 0.61$  as an example. The predictions from the CMB are shown with MCMC samples color-coded by  $H_0$ , which varies fairly monotonically along the degeneracy line set by the angular acoustic scale, corresponding to the peak spacing in the CMB power spectrum. The MCMC samples shown are drawn from the full chains, and include points from the tails of the distributions in addition to high-likelihood samples. The shaded blue contours correspond to the BOSS measurements, which are precise enough to substantially reduce the range of  $H_0$  values allowed by breaking CMB degeneracies. The mixing of colors visible in the ACTPol and SPT panels reflects additional degeneracy between  $H_0$  and other parameters arising from the more limited range of angular scales provided by these data.

In conjunction with the CMB, and in the context of  $\Lambda$ CDM, the BAO have the effect of disfavoring both the higher values of  $H_0$  preferred by the distance ladder, and the lower values preferred by the *Planck* damping tail at  $\ell > 800$ . If we exclude *Planck*, the CMB + BAO values lie  $2.4 - 3.1\sigma$  from the R16 measurement, depending on the choice of CMB dataset. While this trend has been reported before using WMAP data (Planck Collaboration et al. 2016; Bernal et al. 2016), here we show that the measurements of the damping tail from ACT-Pol and SPT produce the same effect even without information from the larger scales measured by the satellite experiments. The fact that combining ACTPol and BAO data produces an  $H_0$  value  $> 3\sigma$  lower than R16 provides strong evidence that the  $H_0$  discrepancy cannot be explained solely by a systematic specific to the *Planck* data. On the other hand, using the difference-covariance method described in Section 4.1 of Planck Collaboration et al. (2016), the shift in  $H_0$  from adding the BAO to the  $\ell > 800$  *Planck* temperature power spectrum is larger than expected at the  $2.2$  and  $2.8\sigma$  level for the  $\tau = 0.07 \pm 0.02$  and  $0.055 \pm 0.009$  priors, respectively.

The CMB + Ly $\alpha$  BAO fits yield higher values of  $H_0$  than the CMB alone, without significantly smaller uncertainties. This reflects the tension between the CMB and Ly $\alpha$  BAO discussed in earlier work (e.g., Delubac et al. 2015; Planck Collaboration et al. 2016). In a joint fit with all the BAO data the Ly $\alpha$  measurements lack the constraining power to overcome the galaxy BAO, and consequently our results are fairly insensitive to whether the Ly $\alpha$  are included along with the galaxy BAO or not. The interaction between the galaxy and Ly $\alpha$  BAO constraints is discussed further in Section 3.3.

<sup>10</sup> <http://cosmologist.info/cosmomc/>

**Table 2**

Constraints on  $H_0$  in the  $\Lambda$ CDM model from the CMB alone and from combining CMB with BAO data, with the significance of the difference from the distance ladder measurement ( $73.24 \pm 1.74$ ; Riess et al. 2016) in parenthesis, assuming uncorrelated Gaussian errors (all values in  $\text{km s}^{-1} \text{Mpc}^{-1}$ )

CMB dataset	Large-scale likelihood <sup>a</sup>	Power spectrum likelihoods <sup>b</sup>	$H_0$ (CMB only)	BAO data <sup>c</sup>	$H_0$ (CMB+BAO)
WMAP 9-year	WMAP	TT, TE, EE	$69.68 \pm 2.17$ (1.3 $\sigma$ )	gal+Ly $\alpha$	$68.30 \pm 0.72$ (2.6 $\sigma$ )
	"	"	"	gal	$68.19 \pm 0.72$ (2.7 $\sigma$ )
	"	"	"	Ly $\alpha$	$71.01 \pm 2.10$ (0.8 $\sigma$ )
ACTPol Two-Season	$\tau = 0.07 \pm 0.02$	TT, TE, EE, $\phi\phi$	$67.12 \pm 2.67$ (1.9 $\sigma$ )	gal+Ly $\alpha$	$67.23 \pm 0.80$ (3.1 $\sigma$ )
	"	"	"	gal	$66.94 \pm 0.77$ (3.3 $\sigma$ )
	"	"	"	Ly $\alpha$	$69.59 \pm 2.61$ (1.3 $\sigma$ )
	"	TT, TE, EE	$67.60 \pm 3.56$ (1.4 $\sigma$ )	gal+Ly $\alpha$	$67.29 \pm 0.83$ (3.1 $\sigma$ )
	$\tau = 0.055 \pm 0.009$	TT, TE, EE, $\phi\phi$	$66.55 \pm 2.59$ (2.1 $\sigma$ )	gal+Ly $\alpha$	$67.21 \pm 0.83$ (3.1 $\sigma$ )
SPT-SZ	$\tau = 0.07 \pm 0.02$	TT, $\phi\phi$	$71.38 \pm 3.09$ (0.5 $\sigma$ )	gal+Ly $\alpha$	$68.52 \pm 0.90$ (2.4 $\sigma$ )
	"	"	"	gal	$68.25 \pm 0.91$ (2.5 $\sigma$ )
	"	"	"	Ly $\alpha$	$73.74 \pm 2.84$ (0.2 $\sigma$ )
	"	TT	$73.20 \pm 3.54$ (0.0 $\sigma$ )	gal+Ly $\alpha$	$68.49 \pm 0.92$ (2.4 $\sigma$ )
	$\tau = 0.055 \pm 0.009$	TT, $\phi\phi$	$70.67 \pm 3.06$ (0.7 $\sigma$ )	gal+Ly $\alpha$	$68.46 \pm 0.88$ (2.5 $\sigma$ )
Planck	lowTEB <sup>d</sup>	plikHM_TT 2015, $\phi\phi$	$67.86 \pm 0.92$ (2.7 $\sigma$ )	gal+Ly $\alpha$	$68.06 \pm 0.56$ (2.8 $\sigma$ )
	"	"	"	gal	$67.95 \pm 0.54$ (2.9 $\sigma$ )
	"	"	"	Ly $\alpha$	$68.17 \pm 0.93$ (2.6 $\sigma$ )
	lowTEB	plikHM_TT 2015	$67.81 \pm 0.92$ (2.8 $\sigma$ )	gal+Ly $\alpha$	$67.97 \pm 0.56$ (2.9 $\sigma$ )
	$\tau = 0.055 \pm 0.009$ , lowl <sup>e</sup>	plikHM_TT 2015	$66.88 \pm 0.91$ (3.2 $\sigma$ )	gal+Ly $\alpha$	$67.72 \pm 0.54$ (3.0 $\sigma$ )
	$\tau = 0.055 \pm 0.009$ , lowl	plikHM_TTTEE 2015	$66.93 \pm 0.62$ (3.4 $\sigma$ )	gal+Ly $\alpha$	$67.53 \pm 0.45$ (3.2 $\sigma$ )
	$\tau = 0.07 \pm 0.02$ , lowl	plikHM_TT $\ell < 800$	$70.08 \pm 1.96$ (1.2 $\sigma$ )	gal+Ly $\alpha$	$68.34 \pm 0.67$ (2.6 $\sigma$ )
	$\tau = 0.055 \pm 0.009$ , lowl	plikHM_TT $\ell < 800$	$69.78 \pm 1.86$ (1.4 $\sigma$ )	gal+Ly $\alpha$	$68.29 \pm 0.66$ (2.7 $\sigma$ )
	$\tau = 0.07 \pm 0.02$	plikHM_TT $\ell > 800$	$65.12 \pm 1.45$ (3.6 $\sigma$ )	gal+Ly $\alpha$	$67.91 \pm 0.66$ (2.9 $\sigma$ )
	$\tau = 0.055 \pm 0.009$	plikHM_TT $\ell > 800$	$64.30 \pm 1.31$ (4.1 $\sigma$ )	gal+Ly $\alpha$	$67.55 \pm 0.62$ (3.1 $\sigma$ )

<sup>a</sup>Pixel-based and other likelihoods used at multipoles  $\ell \lesssim 30$ . For some fits, particularly with the ACTPol and SPT experiments that do not probe these scales, we indicate the Gaussian prior adopted on  $\tau$  instead.

<sup>b</sup>Temperature, E-mode polarization, temperature-polarization cross-spectrum and lensing potential power spectra are denoted TT, EE, TE, and  $\phi\phi$ , respectively.

<sup>c</sup>'gal' refers to galaxy BAO; 'Ly $\alpha$ ' refers to Lyman- $\alpha$  forest and QSO $\times$ Ly $\alpha$  BAO (see Table 1).

<sup>d</sup>lowTEB is the combined temperature-plus-polarization *Planck* likelihood for  $\ell < 30$ .

<sup>e</sup>Since the Planck Collaboration Int. LI (2016) low-multipole polarization likelihood is not publicly available we approximate its inclusion with a prior  $\tau = 0.055 \pm 0.009$ , which produces constraints in very good agreement with their Table 8. lowl is the *Planck* temperature-only likelihood for  $\ell < 30$  (no polarization).

We note that the SPT values in Table 2 differ from the value of  $75.0 \pm 3.5 \text{ km s}^{-1} \text{Mpc}^{-1}$  quoted in Table 3 of the original SPT analysis by Story et al. (2013). This difference is driven by three effects: (i) the inclusion of the SPT lensing  $\phi\phi$  power spectrum measurement from van Engelen et al. (2012) in some of our fits, (ii) the difference in  $\tau$  prior: we used  $0.07 \pm 0.02$  or  $0.055 \pm 0.009$ , while Story et al. (2013) used  $0.088 \pm 0.015$ , and (iii) different CosmoMC versions or fitting options, including the fact that we set the total neutrino mass to 0.06 eV in our fits, while Story et al. (2013) assumed massless neutrinos, which leads to a  $\sim 0.2\sigma$  shift in  $H_0$ . We have verified that if we use the Story et al. (2013) assumptions we reproduce their  $75.0 \pm 3.5$  constraint. Aylor et al. (2017) recently derived parameters from SPT with an updated *Planck*-based calibration and improved likelihood, however the shift they report in  $H_0$  is small and would not meaningfully affect our results.

### 3.2. Angle-averaged versus anisotropic BAO

Bennett et al. (2014; hereafter B14) used pre-*Planck* CMB data along with BAO measurements available at the time (6dFGS, BOSS DR11, including the Ly $\alpha$  but not QSO $\times$ Ly $\alpha$  cross-correlation; we refer to these data

as BAO14) to constrain

$$H_0 = 69.3 \pm 0.7 \text{ km s}^{-1} \text{Mpc}^{-1} \quad (2)$$

(WMAP+ACT+SPT+BAO14).

This value is noticeably higher than the CMB+BAO values reported in Table 2. To make a more direct comparison we performed an updated fit using WMAP, ACTPol, SPT, and the latest BAO data, and find

$$H_0 = 68.34 \pm 0.61 \text{ km s}^{-1} \text{Mpc}^{-1} \quad (3)$$

(WMAP+ACTPol+SPT+BAO).

The difference in these values appears large given the overlap in data sets used and so we investigated this difference in detail. We found that the downward shift in our current fits is due to a combination of several effects:

- (i) The biggest difference comes from using the transverse and line-of-sight BOSS BAO scale measurements now available separately rather than the angle-averaged  $D_V(z)/r_d$  used in B14. Using the BOSS DR11 CMASS anisotropic BAO instead of the BOSS DR11 CMASS angle-averaged BAO shifts the WMAP9+ACT+SPT+BAO14  $H_0$  constraint downwards by  $0.61 \text{ km s}^{-1} \text{Mpc}^{-1}$ , a shift

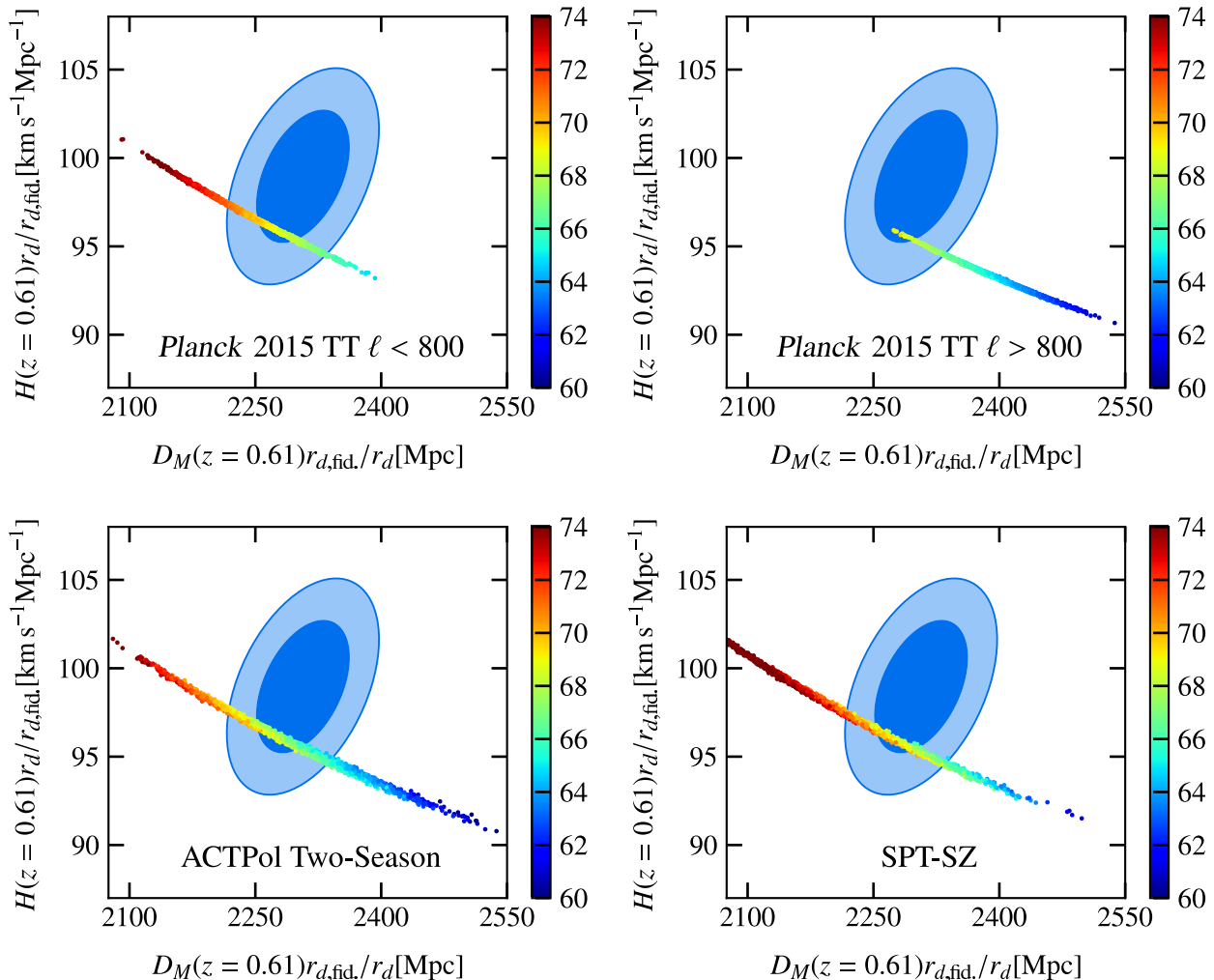


**Figure 1.** Including BAO data substantially tightens CMB constraints on  $H_0$ . The observables corresponding to the transverse and line-of-sight BAO scale,  $D_M r_{d,\text{fid.}}/r_d$ , and  $H r_{d,\text{fid.}}$  (Section 2 and Table 1), are shown for redshift  $z = 0.61$ . The blue shaded contours are the measurements from the final BOSS DR12 analysis (Alam et al. 2017). The different panels contain predictions from different, essentially independent, CMB measurements assuming a flat  $\Lambda$ CDM model, with MCMC samples color-coded by  $H_0$  in  $\text{km s}^{-1} \text{Mpc}^{-1}$ . The same  $\tau = 0.07 \pm 0.02$  prior is used in each case. The addition of the BAO tightens the  $H_0$  constraint by more than a factor of three in the case of ACTPol or SPT data (Table 2). When combined with *any* current CMB data set the galaxy BAO disfavor the values of  $H_0$  preferred by the distance ladder ( $73.24 \pm 1.74 \text{ km s}^{-1} \text{Mpc}^{-1}$ ; Riess et al. 2016) at moderate to high significance. The lower values preferred by the high-multipole *Planck* data (the constraint from the samples shown in the top-right panel is  $65.12 \pm 1.45 \text{ km s}^{-1} \text{Mpc}^{-1}$ ) are also disfavored.

comparable to the total uncertainty. This is discussed in more detail below.

- (ii) A smaller shift of around  $0.2 \text{ km s}^{-1} \text{Mpc}^{-1}$  is due to different likelihood codes. We find  $H_0 = 69.07 \pm 0.70 \text{ km s}^{-1} \text{Mpc}^{-1}$  using WMAP9+ACT+SPT+BAO14. Our results were obtained with the November 2016 versions of CAMB<sup>11</sup> and CosmoMC, while a different MCMC code was used in B14. Furthermore, our implementation of the DR11 Ly $\alpha$  BAO constraint uses the  $\chi^2$  look-up tables provided by BOSS<sup>12</sup>, whereas B14 constructed a likelihood directly from values reported by Delubac et al. (2015).

- (iii) The ACTPol data have a stronger downward pull on  $H_0$  than ACT. Both ACT and ACTPol prefer a lower  $H_0$  value than WMAP alone (Sievers et al. 2013; Louis et al. 2017). The SPT data prefer a higher  $H_0$  value than WMAP, and this preference wins out in the combination with ACT. With ACTPol, however, the downward pull is stronger, and the resulting constraint shifts downwards from  $69.98 \pm 1.58$  (WMAP9+ACT+SPT) to  $69.08 \pm 1.37 \text{ km s}^{-1} \text{Mpc}^{-1}$  (WMAP+ACTPol+SPT). In combination with the BAO the impact of using ACTPol instead of ACT is subdominant to the choice of BAO constraints.

- (iv) The SDSS MGS BAO constraint at  $z_{\text{eff}} = 0.15$  was not used by B14. While the MGS measurement has lower precision than BOSS (4% compared to

<sup>11</sup> <http://camb.info/>

<sup>12</sup> <http://darkmatter.ps.uci.edu/baofit/>

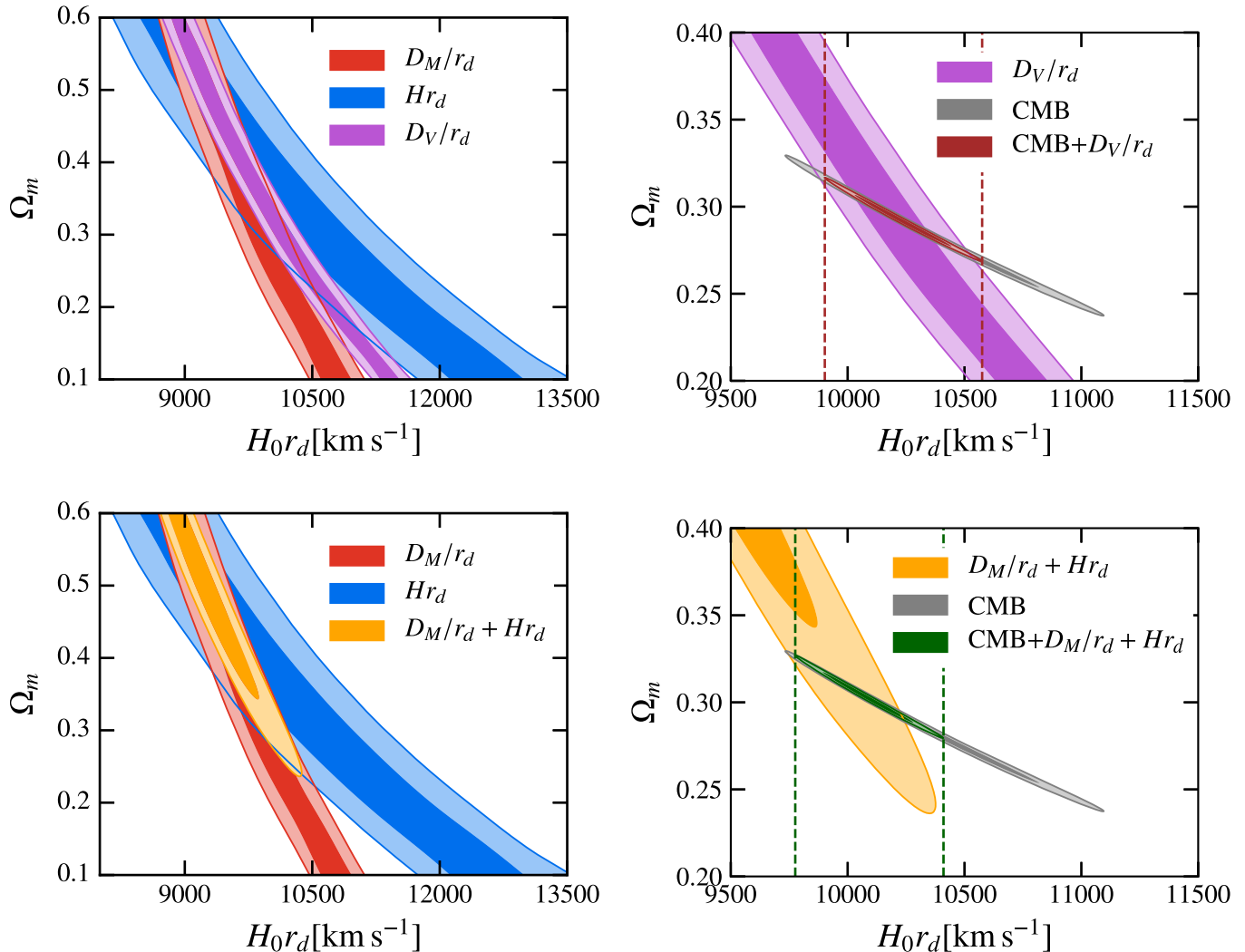


**Figure 2.** Use of the angle-averaged BAO constraint,  $D_V(z)/r_d$ , instead of the full anisotropic information,  $D_M(z)/r_d$  plus  $H(z)r_d$ , can impact determination of  $H_0$  from combined CMB+BAO fits. The upper left panel shows constraints from the same BOSS CMASS DR11 galaxy sample at  $z_{\text{eff}} = 0.57$  (Anderson et al. 2014) but different BAO measures – transverse ( $D_M/r_d$ ), line-of-sight ( $Hr_d$ ), and angle-averaged ( $D_V/r_d$ , see Section 2.1). The lower left panel shows the anisotropic constraint from combining  $D_M(z)/r_d$  and  $H(z)r_d$ . While there is significant overlap between the angle-averaged and anisotropic contours, the angle-averaged contour extends to lower values of  $\Omega_m$ , which are not allowed by the anisotropic constraint. The upper right and lower right panels show the effect of adding the BAO information to CMB data (we show the same data sets used by Bennett et al. 2014, WMAP+ACT+SPT). The use of the angle-averaged  $D_V(z)/r_d$  constraint diminishes the downward pull on  $H_0 r_d$ , and also  $H_0$ , from the BAO. The vertical dashed lines correspond to the bounds of the contours containing 95% of the CMB+BAO MCMC samples.

around 1%), it also has a stronger preference for lower  $H_0$  in conjunction with the CMB data.

Why does the choice of anisotropic or angle-averaged BOSS CMASS BAO make such a large difference given the same galaxy sample is used for each? In the flat  $\Lambda$ CDM model, all the information from any BAO measurement is contained in contours in the two-dimensional  $\Omega_m - H_0 r_d$  space (Addison et al. 2013). The relative late-time expansion history is determined by  $\Omega_m$ , with  $\Omega_\Lambda$  determined implicitly by the flatness constraint. The impact of radiation on the late-time expansion is small enough compared to the precision of current BAO measurements that uncertainties in the CMB temperature, which constrains the physical density  $\Omega_r h^2$ , or in converting to the fractional density,  $\Omega_r$ , can be neglected. The combination  $H_0 r_d$  provides an overall normalization

factor and reflects the fact that the absolute length of the sound horizon, and a change in the normalization of the expansion rate, are completely degenerate when only fitting to measurements of the BAO scale.

The upper left and lower left panels of Figure 2 shows constraints in the  $\Omega_m - H_0 r_d$  plane for the DR11 BOSS CMASS sample at  $z_{\text{eff}} = 0.57$  (Anderson et al. 2014). We show the transverse ( $D_M/r_d$ ) and line-of-sight ( $Hr_d$ ) contours separately, as well as the contour from combining both, and the angle-averaged  $D_V(z)/r_d$  contour. While there is substantial overlap between the combined anisotropic contour and the  $D_V(z)/r_d$  contour, a portion of the parameter space is allowed by  $D_V(z)/r_d$  but ruled out by the combined anisotropic measurements. This portion is relevant when the BAO and CMB are combined, as shown in the upper right and lower right panels

of Figure 2, with the anisotropic  $D_M(z)/r_d + H(z)r_d$  constraint pulling down more strongly on  $H_0 r_d$ , and hence  $H_0$ , since  $H_0$  and  $r_d$  are only partially degenerate in the CMB. The same effect is apparent in Figure 8 of Cuesta et al. (2016).

We conclude that the shift in  $H_0$  from using the angle-averaged  $D_V(z)/r_d$  instead of the full anisotropic BAO information is not caused by an inconsistency in the BAO measurements, but instead due to the compression of information inherent to  $D_V(z)/r_d$ . It is therefore preferable to use the anisotropic constraints where possible.

### 3.3. Constraints from the BAO scale alone

We now consider constraints from the BAO data without the strong additional constraining power of the CMB anisotropy measurements. As discussed above, in the flat  $\Lambda$ CDM model, BAO measurements provide contours in the  $\Omega_m - H_0 r_d$  plane. Combining the galaxy and Ly $\alpha$  BAO provides a tight constraint on  $\Omega_m$  from the late-time expansion history, even when marginalizing over the normalization  $H_0 r_d$ . For the BAO listed in Table 1 we find constraints of

$$\begin{aligned} \Omega_m &= 0.292 \pm 0.020 \\ H_0 r_d &= (10119 \pm 138) \text{ km s}^{-1}. \end{aligned} \quad (4)$$

The left panel of Figure 3 shows constraints from the galaxy and Ly $\alpha$  BAO in the  $\Omega_m - H_0 r_d$  plane. The orientation of these contours can be approximately understood from considering the redshift dependence of  $H(z)$ . Similar arguments hold for  $D_A(z)$ . At the Ly $\alpha$  BAO redshifts the universe is matter dominated, and  $H(z) \simeq H_0 \Omega_m^{1/2} (1+z)^{3/2}$ , so that  $H(z)r_d$  constraints produce contours along the direction with  $H_0 r_d \cdot \Omega_m^{1/2}$  roughly constant. At lower redshifts, where dark energy becomes dominant,  $H(z)$  depends less strongly on  $\Omega_m$ , leading to the galaxy BAO contour being oriented more along the direction of the y-axis in Figure 3<sup>13</sup>. There is little overlap between the galaxy and Ly $\alpha$  contours. To quantify this difference, we consider the test described in Section 4.1 of Hou et al. (2014). We calculate  $\Delta\chi^2 = \chi_{X+Y}^2 - \chi_X^2 - \chi_Y^2$ , where in this case  $X$  and  $Y$  are the galaxy and Ly $\alpha$  BAO data, respectively,  $\chi_{X+Y}^2$  denotes the best-fit  $\chi^2$  from the joint fit, and  $\chi_X^2$  and  $\chi_Y^2$  are the best-fit  $\chi^2$  from the fits to just the galaxy or just the Ly $\alpha$  data. For Gaussian-distributed data<sup>14</sup>, if  $X$  and  $Y$  are independent and  $\Lambda$ CDM is the correct model then  $\Delta\chi^2$  is drawn from a  $\chi^2$  distribution with  $N_{\Delta\chi^2} = N_{X+Y} - N_X - N_Y$  degrees of freedom (dof). We find

$$\begin{aligned} \chi_{\text{gal}}^2 &= 2.98 & N_{\text{gal}} &= 8 - 2 = 6 \\ \chi_{\text{Ly}\alpha}^2 &= 0.92 & N_{\text{Ly}\alpha} &= 4 - 2 = 2 \\ \chi_{\text{gal+Ly}\alpha}^2 &= 13.63 & N_{\text{gal+Ly}\alpha} &= 12 - 2 = 10 \\ \Delta\chi^2 &= 9.73 & N_{\Delta\chi^2} &= 10 - 6 - 2 = 2 \end{aligned}$$

The probability to exceed (PTE) for  $\chi^2 = 9.73$  with  $N_{\text{dof}} = 2$  is  $7.71 \times 10^{-3}$ , which corresponds to a 2.4 $\sigma$

<sup>13</sup> If BAO measurements at  $z = 0$  were possible they would produce exactly vertical contours in Figure 3.

<sup>14</sup> This is a reasonable approximation when the Ly $\alpha$  and QSO $\times$ Ly $\alpha$  BAO are combined (Delubac et al. 2015).

disagreement. This is comparable to the 2.5 $\sigma$  tension reported between the Ly $\alpha$  BAO and *Planck* measurements by Delubac et al. (2015). As discussed by Aubourg et al. (2015), modifying the cosmological model to improve three-way agreement between CMB, galaxy BAO, and Ly $\alpha$  BAO appears difficult. Here we note that the combined contour in Figure 3 lies at the intersection of the main degeneracy directions determined by the redshift coverage of the galaxy and Ly $\alpha$  measurements. If future data shift the galaxy or Ly $\alpha$  BAO constraints *along* these degeneracy lines (as opposed to perpendicular to them) the main result would be to change the quality of the combined fit rather than changing the parameter values. We further note that the matter density reported in (4) is in agreement with the value of  $0.295 \pm 0.034$  from a joint analysis of type Ia SNe from several surveys covering  $0 < z < 1$ , completely independent of LSS clustering (Betoule et al. 2014). This is illustrated in the right panel of Figure 3, which shows a comparison of BAO, WMAP 9-year, *Planck* 2016<sup>15</sup>, and SNe constraints on  $\Omega_m$  for the flat  $\Lambda$ CDM model.

### 3.4. Constraining $H_0$ with BAO plus deuterium abundance in $\Lambda$ CDM

Obtaining a constraint on  $H_0$  from the BAO requires adding information to break the  $H_0 - r_d$  degeneracy. One way to do this is to add a constraint on the baryon density (e.g., Addison et al. 2013; Aubourg et al. 2015; Wang et al. 2017). We assume that the photon energy density, or, equivalently, the CMB mean temperature, is also known. The CMB temperature was measured precisely by *COBE*/FIRAS (Fixsen et al. 1996; Fixsen 2009) and we view this result as independent of the CMB anisotropy measurements performed by more recent experiments. Note that while the  $H_0$  in the  $H(z)$  in the denominator of (1) cancels in the  $H_0 r_d$  product, some residual  $H_0$  dependence still exists because the decoupling redshift and the sound speed depend on the *physical* matter and radiation densities,  $\Omega_m h^2$  and  $\Omega_r h^2$ , respectively, while the expansion rate  $H(z)$  depends on the *fractional* densities  $\Omega_m$  and  $\Omega_r$ .

In the BAO fit with an external baryon density prior,  $\Omega_m$  performs double duty. It not only goes into determining the late-time expansion ( $D_M$  and  $H$  at the BAO survey redshifts) but also controls the expansion history in the early universe prior to baryons decoupling from photons, since the photon and neutrino properties (with  $N_{\text{eff}} = 3.046$ ) are held fixed. As well as providing an indirect  $H_0$  constraint, the BAO+ $\Omega_b h^2$  fit also serves as something of a self-consistency test of early and late-time expansion.

The most precise constraints on  $\Omega_b h^2$  independent of the CMB power spectrum come from estimates of the primordial deuterium abundance. In standard Big Bang nucleosynthesis (BBN), the abundance of light nuclei is determined by a single parameter, the baryon-to-photon ratio  $\eta$  (see recent review by Cyburt et al. 2016, and references therein). Taking the photon number density as fixed from the CMB temperature, a measurement of the primordial deuterium abundance in conjunction with

<sup>15</sup> We refer to the combination of the 2015 TT constraints with updated  $\tau = 0.055 \pm 0.009$  prior from Planck Collaboration Int. LI (2016) as ‘*Planck* 2016’.



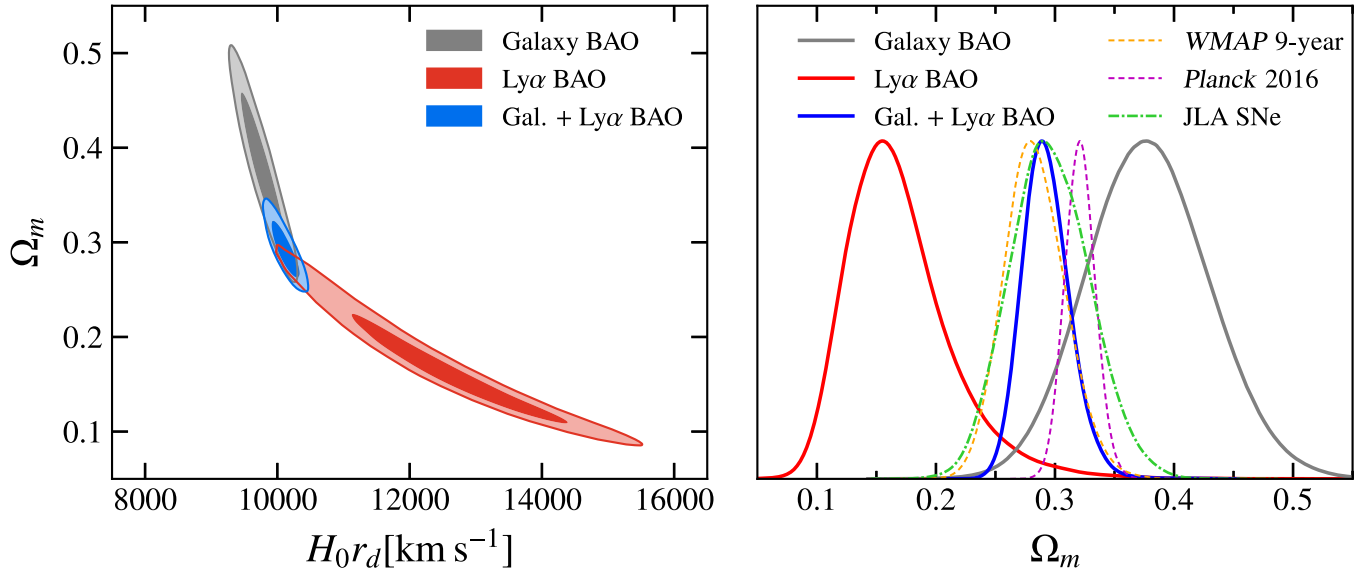


**Figure 3.** *Left:* Comparison of BAO-only constraints in the flat  $\Lambda$ CDM model. Contours containing 68 and 95% of MCMC samples are shown for galaxy ( $z_{\text{eff}} \leq 0.61$ ) and Ly $\alpha$  forest ( $z_{\text{eff}} \geq 2.3$ ) BAO separately and in a joint fit using the BAO data listed in Table 1. In flat  $\Lambda$ CDM the late-time expansion rate is determined only by  $\Omega_m$ , with  $H_0 r_d$  acting as an overall expansion normalization. *Right:* Comparison of  $\Omega_m$  constraints from BAO, CMB and SNe measurements. The SNe constraint is from the “joint light-curve analysis” (JLA) presented by Betoule et al. (2014). While the combined BAO fit produces a tight constraint  $\Omega_m = 0.293 \pm 0.020$ , in agreement with the CMB and SNe determinations, there is a  $2.4\sigma$  tension between the galaxy and Ly $\alpha$  BAO, which individually prefer higher and lower values of  $\Omega_m$ , respectively.

**Table 3**

$\Lambda$ CDM constraints from the BAO+D/H fits, using either the theoretical or empirical  $d(p, \gamma)^3\text{He}$  reaction rate, with CMB anisotropy constraints from WMAP and Planck included for comparison

Parameter	BAO+D/H (theoretical)	BAO+D/H (empirical)	WMAP 9-year	Planck 2016
$100\Omega_b h^2$	$2.156 \pm 0.020$	$2.257 \pm 0.034$	$2.265 \pm 0.049$	$2.215 \pm 0.021$
$100\Omega_c h^2$	$10.94 \pm 1.20$	$11.19 \pm 1.29$	$11.37 \pm 0.46$	$12.07 \pm 0.21$
$100\theta_{\text{MC}}$	$1.0292 \pm 0.0168$	$1.0320 \pm 0.0173$	$1.04025 \pm 0.00223$	$1.04076 \pm 0.00047$
$H_0$ [km s $^{-1}$ Mpc $^{-1}$ ]	$66.98 \pm 1.18$	$67.81 \pm 1.25$	$69.68 \pm 2.17$	$66.89 \pm 0.90$
$\Omega_m$	$0.293 \pm 0.019$	$0.293 \pm 0.020$	$0.283 \pm 0.026$	$0.321 \pm 0.013$
$r_d$ [Mpc]	$151.6 \pm 3.4$	$149.2 \pm 3.6$	$148.49 \pm 1.23$	$147.16 \pm 0.48$

knowledge of BBN physics provides a constraint on  $\Omega_b h^2$ . Precise estimates of the primordial deuterium abundance have been made in recent years using extremely metal-poor damped Lyman- $\alpha$  (DLA) systems along sight lines to high-redshift quasars (e.g., Pettini & Cooke 2012; Cooke et al. 2014, 2016; Riemer-Sørensen et al. 2017). Cooke et al. (2016; hereafter C16) report

$$10^5 \text{D}_I/\text{H}_I = 2.547 \pm 0.033 \quad (5)$$

by combining six such systems. The  $d(p, \gamma)^3\text{He}$  reaction rate plays a key role in the conversion from D/H to  $\Omega_b h^2$ . Using the theoretical calculation for this rate from Marucci et al. (2016), C16 find

$$100\Omega_b h^2 = 2.156 \pm 0.020 \quad (6)$$

(D/H, theoretical),

which is  $> 2\sigma$  lower than the Planck value (assuming a standard  $\Lambda$ CDM model throughout). Using instead an empirically derived  $d(p, \gamma)^3\text{He}$  rate, C16 find

$$100\Omega_b h^2 = 2.260 \pm 0.034 \quad (7)$$

(D/H, empirical rate),

which has a larger uncertainty but is in better agreement with CMB-derived values. We performed fits to the galaxy plus Ly $\alpha$  BAO data with the addition of each of the Gaussian priors on  $\Omega_b h^2$  in (6) and (7) in turn. We show parameter constraints in Table 3, including the WMAP 9-year and Planck 2016 CMB anisotropy constraints for comparison.

In the BAO+D/H fits,  $\Omega_b h^2$  is driven solely by the D/H prior, as expected, and  $\Omega_m$  matches the BAO-only value. While the choice of the  $d(p, \gamma)^3\text{He}$  reaction rate significantly impacts the value of  $\Omega_b h^2$ , it has a reduced impact on the inferred  $H_0$ , because  $r_d$  only depends weakly on  $\Omega_b h^2$  (Eisenstein & Hu 1998; Addison et al. 2013). Specifically, replacing the theoretical rate with the empirical one shifts the center of the  $\Omega_b h^2$  distribution by 5.2 times the original uncertainty, but shifts the  $H_0$  distribution by only 0.7 times the original uncertainty. Our BAO+D/H results for  $H_0$  are more robust to the choice of rate than one might expect from the  $\Omega_b h^2$  difference.

The  $H_0$  values listed in Table 3 from the BAO+D/H fits have uncertainties of around 1.8% and are 3.0 and  $2.5\sigma$  lower than the R16 distance ladder value of  $73.24 \pm$

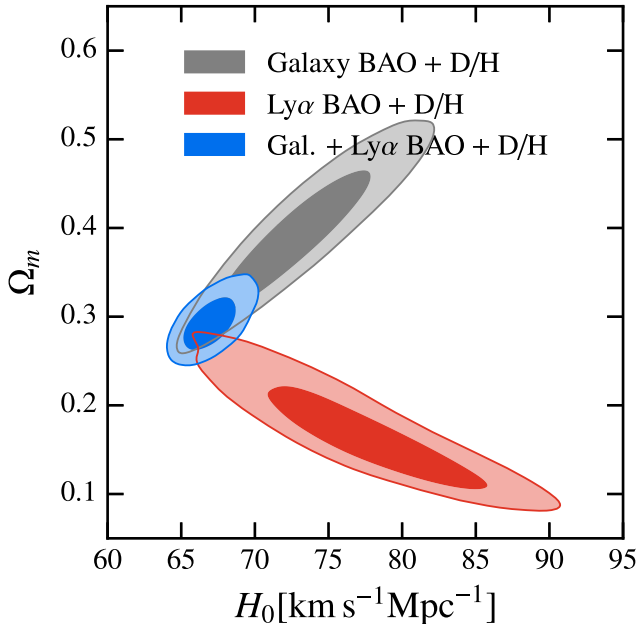


**Figure 4.** Adding an estimate of the baryon density,  $\Omega_b h^2$ , in this case from deuterium abundance (D/H) measurements, breaks the BAO  $H_0 - r_d$  degeneracy in  $\Lambda$ CDM. The same contours are shown as in Figure 3, with the addition of a Gaussian prior  $100\Omega_b h^2 = 2.156 \pm 0.020$  (Cooke et al. 2016). In contrast to Figure 3, here  $\Omega_m$  determines both the early time expansion, including the absolute sound horizon,  $r_d$ , as well as the late-time expansion history. The radiation density is fixed from COBE/FIRAS CMB mean temperature measurements. The combined BAO+D/H constraint,  $H_0 = 66.98 \pm 1.18 \text{ km s}^{-1} \text{ Mpc}^{-1}$  is  $3.0\sigma$  lower than the Riess et al. (2016) distance ladder determination and is independent of CMB anisotropy data.

$1.74 \text{ km s}^{-1} \text{ Mpc}^{-1}$  for the theoretical and empirical  $d(p, \gamma)^3\text{He}$  rates, respectively. The combination of precise BAO and D/H measurements enables determinations of  $H_0$  within the context of the flat  $\Lambda$ CDM model that are almost 50% tighter than the distance ladder measurement, and lower at moderate to strong significance. We emphasize that these constraints are completely independent of CMB anisotropy measurements.

Constraints in the  $\Omega_m - H_0$  plane for the BAO+D/H fits with the theoretical  $d(p, \gamma)^3\text{He}$  rate are shown in Figure 4. We show results from the galaxy and Ly $\alpha$  BAO separately and together, as before. Tension between the galaxy and Ly $\alpha$  BAO is again apparent. Adding D/H to these data separately favors higher values of  $H_0$ , and it is only when galaxy and Ly $\alpha$  BAO are combined that  $H_0$  is constrained to the values quoted in Table 3.

The direction of the Ly $\alpha$  BAO contour is roughly the same in the left panel of Figure 3 and in Figure 4, while that of the galaxy BAO contour changes. This behavior can be understood by considering how  $r_d$  depends on  $\Omega_m$  and  $H_0$ . For a given value of  $\Omega_b h^2$ ,  $r_d$  depends approximately on the combination  $H_0 \cdot \Omega_m^{1/2}$  (equation 26 of Eisenstein & Hu 1998). This is the same dependence as  $H(z)$  at the Ly $\alpha$  redshifts (Section 3.3) and is related to the fact that the universe is largely matter dominated in both cases. The dependence of  $H(z)$  on  $\Omega_m$  at the galaxy BAO redshifts is weaker, and the direction of the galaxy BAO contour in Figure 4 is approximately deter-

mined by requiring  $H_0 r_d$  to be roughly constant as  $\Omega_m$  varies. This produces a positive correlation between  $H_0$  and  $\Omega_m$  because  $r_d$  decreases as  $H_0 \Omega_m^{1/2}$  increases.

For the BAO+D/H fits, we ran COSMOMC as one would when fitting to the CMB: the fitted parameters are  $\Omega_b h^2$ , the physical cold dark matter density,  $\Omega_c h^2$ , and the angular sound horizon,  $\theta_{\text{MC}}$ , and  $H_0$ ,  $\Omega_m$ , and  $r_d$  are derived from these three. Since the BAO+D/H data are insensitive to the amplitude and tilt of the primordial power spectrum, and the optical depth to reionization, these other  $\Lambda$ CDM parameters are held fixed. Consistent results were obtained using earlier BAO and D/H data by Addison et al. (2013) and Aubourg et al. (2015). We note that Riemer-Sørensen & Sem Jensen (2017) recently obtained a tighter constraint on D/H than we have used here by combining the DLAs used by C16 with a number of additional measurements. Using this tighter constraint would not impact our conclusions.

### 3.5. BAO and light element abundance constraints with varying $N_{\text{eff}}$

In the  $\Lambda$ CDM+ $N_{\text{eff}}$  model, there is a perfect degeneracy between  $\Omega_b h^2$  and  $N_{\text{eff}}$  from D/H measurements (Fig. 6 of C16). Closed contours in the  $\Omega_b h^2 - N_{\text{eff}}$  plane can be obtained from combining estimates of the primordial D/H and  $^4\text{He}$  abundance (e.g., review by Cyburt et al. 2016, and references therein). The primordial  $^4\text{He}$  abundance is estimated from He and H emission lines in extragalactic HII regions. Obtaining accurate constraints is challenging due to dependence on environmental parameters such as temperature, electron density, and metallicity, which must be modeled. An important recent development is the use of the HeI line at 10830 Å to help break modeling degeneracies (Izotov et al. 2014). The value of the primordial helium fraction reported by Izotov et al. (2014),  $Y_p = 0.2551 \pm 0.0022$ , is, however, significantly higher than values found in some subsequent analyses of the same HII sample using different selection criteria and fitting methodology. For example, Aver et al. (2015) found  $Y_p = 0.2449 \pm 0.0040$ , while Peimbert et al. (2016) found  $Y_p = 0.2446 \pm 0.0029$ . The different  $Y_p$  values lead to significantly different inferences for  $N_{\text{eff}}$  when used in combination with D/H or CMB power spectra measurements. Izotov et al. (2014) found evidence for additional neutrino species at 99% confidence, while, for instance, Cyburt et al. (2016) report  $N_{\text{eff}} = 2.85 \pm 0.28$ , and Peimbert et al. (2016) found  $N_{\text{eff}} = 2.90 \pm 0.22$ , consistent with the standard model value of 3.046.

Current D/H and  $^4\text{He}$  constraints clearly have the *precision* to weigh in significantly on the question of whether allowing  $N_{\text{eff}} > 3$  is effective at resolving  $\Lambda$ CDM tensions. Given the spread in  $Y_p$  values discussed above, and the impact of the choice of  $d(p, \gamma)^3\text{He}$  rate when  $N_{\text{eff}}$  is allowed to vary (Section 5.2 of C16), we do not present a full set of results including BAO and light element abundance data for  $\Lambda$ CDM+ $N_{\text{eff}}$ . Instead we note that combining BAO measurements with D/H and  $^4\text{He}$  constraints on  $N_{\text{eff}}$  that are consistent with the standard model value would produce  $H_0$  values consistent with the values in Table 3, although with larger uncertainties, while higher values of  $N_{\text{eff}}$  would produce a higher  $H_0$ , improving agreement with the distance ladder. The BAO measurements, being only sensitive to  $H_0 r_d$ , and not to

$H_0$  or  $N_{\text{eff}}$  directly, are unable to discriminate between these possibilities.

#### 4. DISCUSSION

We have presented evidence for a lower  $H_0$  value than measured by the local distance ladder that is independent of *Planck*, both from combining BAO with other CMB datasets (*WMAP*, *ACTPol* and *SPT*), and from joint fits to BAO and D/H measurements, within the context of the standard  $\Lambda$ CDM model. In light of this analysis it is clear that the  $H_0$  tension cannot be resolved solely through a systematic error specific to the *Planck* data. It should be noted, however, that it is not simply a case of having a ‘high’  $H_0$  from the distance ladder, and a ‘low’  $H_0$  from *Planck* and the joint BAO fits. The high-multipole *Planck* temperature data prefer  $H_0$  values that are even lower than the CMB+BAO or BAO+D/H values (bottom two rows of Table 2 and top right panel of Fig. 1). Restricting the *Planck* temperature power spectrum to multipoles  $\ell > 800$  produces

$$H_0 = 65.12 \pm 1.45 \text{ km s}^{-1} \text{ Mpc}^{-1} \quad (8)$$

*(Planck 2015 TT  $\ell > 800$ ,  $\tau = 0.07 \pm 0.02$ ),*

or

$$H_0 = 64.30 \pm 1.31 \text{ km s}^{-1} \text{ Mpc}^{-1} \quad (9)$$

*(Planck 2015 TT  $\ell > 800$ ,  $\tau = 0.055 \pm 0.009$ ),*

depending on the choice of  $\tau$  prior. These values are not only in strong tension with R16, but are in moderate tension with some of the CMB+BAO values reported in Table 2. For example, for  $\tau = 0.055 \pm 0.009$ , the SPT+BAO value is lower than R16 by  $2.5\sigma$ , but the *Planck*  $\ell > 800$  value is  $2.6\sigma$  lower again than SPT+BAO. The shift in  $H_0$  from adding the BAO to the  $\ell > 800$  *Planck* constraints is also larger than expected given the improvement in precision, as discussed in Section 3.1. Some  $H_0$  tension remains even if we do not consider the distance ladder constraints. In fact, concordance cannot be achieved through the removal of *any* single data set (e.g., BAO, CMB, distance ladder, or D/H). This is part of the reason the  $H_0$  discrepancy is challenging to resolve: a convincing solution must simultaneously address multiple avenues of disagreement.

A wide range of fits to expanded cosmological models, with various combinations of data, have been presented in recent years to try to reconcile  $H_0$  and other parameter tensions. Our fits in this paper have been restricted to the standard flat  $\Lambda$ CDM model, partly because our results for expanded models would be similar to those already presented by Planck Collaboration et al. (2016), Alam et al. (2017), Heavens et al. (2017), and others. The BAO, CMB, and light element abundance measurements have some common dependence on the early universe expansion history, which makes allowing freedom in, for example,  $N_{\text{eff}}$ , seem attractive. As discussed in Section 1, varying  $N_{\text{eff}}$  does not sufficiently relieve tensions and is not statistically favored over standard  $\Lambda$ CDM for the current BAO, CMB, and distance ladder data. There are good prospects for tightening  $N_{\text{eff}}$  constraints through improved measurements of the high- $\ell$  CMB damping tail in E-mode polarization (e.g., Abazajian et al. 2015, 2016). Future BAO data, for example from the Dark Energy Spectroscopic Instrument

(DESI<sup>16</sup>), Euclid<sup>17</sup>, and WFIRST<sup>18</sup>, will also provide significant improvements in precision over current measurements (for BAO+ $\Omega_b h^2$  forecasts for  $H_0$ , see Wang et al. 2017).

#### 5. CONCLUSIONS

We have examined the role of BAO measurements in determining  $H_0$ . While the BAO data alone are unable to distinguish between a change in  $H_0$  and a change in the absolute sound horizon at decoupling,  $r_d$ , this degeneracy is broken, and a precise  $H_0$  value obtained, when BAO are combined with either CMB power spectra or deuterium abundance measurements. Overall we find convincing evidence for a lower  $H_0$  in  $\Lambda$ CDM than obtained from the latest local distance ladder measurement ( $73.24 \pm 1.74 \text{ km s}^{-1} \text{ Mpc}^{-1}$ ; Riess et al. 2016) even without using data from *Planck*. The motivation and results of this study are summarized as follows:

- (i) Tension at the  $> 3\sigma$  level exists between determinations of  $H_0$  from the distance ladder and the CMB anisotropy measurements from *Planck*, within the context of the standard flat  $\Lambda$ CDM model. Other tensions also exist, for example between *Planck* data and constraints on the growth of structure from some weak lensing surveys.
- (ii) None of the cosmological modifications commonly proposed appear to provide a statistically compelling solution to these tensions, although some, such as allowing freedom in the number of effective relativistic species,  $N_{\text{eff}}$ , do reduce the  $H_0$  disagreement.
- (iii) Combining BAO measurements with CMB power spectrum data from *WMAP*, *ACTPol*, or *SPT*, produces  $H_0$  values lower than the distance ladder by  $2.4 - 3.1\sigma$ , independent of *Planck* (Table 2). The difference was less pronounced in some earlier analyses because of using the angle-averaged BOSS CMASS BAO measurement. The angle-averaged  $D_V(z)/r_d$  constraint is a compression of information and allows a region of parameter space that is ruled out by the full anisotropic BAO constraints (Fig. 2). Adding the BAO improves the  $H_0$  constraint from *ACTPol* or *SPT* by more than a factor of three, making their precision comparable to the *Planck*-only results.
- (iv) Combining BAO data with primordial deuterium (D/H) abundance estimates from metal-poor DLA systems produces precise  $H_0$  values lower than the distance ladder by  $2.5 - 3.0\sigma$ , depending on assumptions about the  $d(p, \gamma)^3\text{He}$  reaction rate (e.g.,  $66.98 \pm 1.18 \text{ km s}^{-1} \text{ Mpc}^{-1}$  for the theoretical rate, see Table 3). This result is independent of any CMB anisotropy measurement and relies only on the CMB mean temperature from *COBE*/FIRAS.
- (v) The two previous results taken together indicate that it is not possible to resolve the  $H_0$  disagree-

<sup>16</sup> <http://desi.lbl.gov/>

<sup>17</sup> <https://www.euclid-ec.org/>

<sup>18</sup> <https://wfirst.gsfc.nasa.gov/>

ment solely through some systematic error specific to the *Planck* data set.

- (vi) The *Planck* high-multipole ( $\ell > 800$ ) damping tail measurements prefer lower values of  $H_0$  than the combined BAO fits, for example  $65.12 \pm 1.45$  and  $64.30 \pm 1.31 \text{ km s}^{-1} \text{ Mpc}^{-1}$ , for  $\tau = 0.07 \pm 0.02$  and  $\tau = 0.055 \pm 0.009$ , respectively. The shift in  $H_0$  from adding the BAO to these data is larger than expected at the 2.2 and  $2.8\sigma$  level for these  $\tau$  priors. The  $H_0$  disagreement is not as simple as the distance ladder value being ‘high’ and other constraints coming out ‘low’, and cannot be resolved through the removal of any single data set.
- (vii) We note that a  $2.4\sigma$  tension exists between the galaxy ( $z \leq 0.61$ ) and  $\text{Ly}\alpha$  ( $z \geq 2.4$ ) BAO, as previously discussed by Aubourg et al. (2015). The BAO+D/H constraints rely on combining these measurements and as such it is important to review their consistency with future data.

In recent years new precise measurements have led to multiple tensions, particularly in  $H_0$ , that are uncomfortably large to be explained by statistical scatter within the context of the standard  $\Lambda\text{CDM}$  model. Whether this is the sign of new physics or underestimated uncertainties, or some combination of effects, remains unclear, and no straightforward explanation has yet presented itself. Near-term improvements in CMB, LSS, and distance ladder data are expected, however continuing to scrutinize existing measurements, as we have in this work, could also prove important in moving towards an eventual resolution.

This research was supported in part by NASA grants NNX15AJ57G, NNX16AF28G, and NNX17AF34G, and JPL grant 1563692, and by the Canadian Institute for Advanced Research (CIFAR). We acknowledge the use of the Legacy Archive for Microwave Background Data Analysis (LAMBDA), part of the High Energy Astrophysics Science Archive Center (HEASARC). HEASARC/LAMBDA is a service of the Astrophysics Science Division at the NASA Goddard Space Flight Center. This work was partly based on observations obtained with *Planck* (<http://www.esa.int/Planck>), an ESA science mission with instruments and contributions directly funded by ESA Member States, NASA, and Canada. Part of this research project was conducted using computational resources at the Maryland Advanced Research Computing Center (MARCC).

The authors would like to thank Erminia Calabrese, Antony Lewis, James Rich, Adam Riess, and Ashley Ross for helpful discussions and clarifications regarding data sets and software used in this work, and we are also grateful to Adam Riess for reading a draft of the manuscript and providing useful suggestions. We acknowledge the use of the *GetDist* plotting package<sup>19</sup>.

## REFERENCES

- Abazajian, K. N., Arnold, K., Austermann, J., et al. 2015, *Astroparticle Physics*, 63, 66
- Abazajian, K. N., Adshead, P., Ahmed, Z., et al. 2016, ArXiv e-prints, arXiv:1610.02743
- Addison, G. E., Hinshaw, G., & Halpern, M. 2013, *MNRAS*, 436, 1674
- Addison, G. E., Huang, Y., Watts, D. J., et al. 2016, *ApJ*, 818, 132
- Alam, S., Ata, M., Bailey, S., et al. 2017, *MNRAS*, 470, 2617
- Alsing, J., Heavens, A., & Jaffe, A. H. 2017, *MNRAS*, 466, 3272
- Anderson, L., Aubourg, É., Bailey, S., et al. 2014, *MNRAS*, 441, 24
- Ata, M., Baumgarten, F., Bautista, J., et al. 2017, ArXiv e-prints, arXiv:1705.06373
- Aubourg, É., Bailey, S., Bautista, J. E., et al. 2015, *Phys. Rev. D*, 92, 123516
- Aver, E., Olive, K. A., & Skillman, E. D. 2015, *J. Cosmology Astropart. Phys.*, 7, 011
- Aylor, K., Hou, Z., Knox, L., et al. 2017, ArXiv e-prints, arXiv:1706.10286
- Bautista, J. E., Busca, N. G., Guy, J., et al. 2017, *A&A*, 603, A12
- Bennett, C. L., Larson, D., Weiland, J. L., & Hinshaw, G. 2014, *ApJ*, 794, 135
- Bennett, C. L., Larson, D., Weiland, J. L., et al. 2013, *ApJS*, 208, 20
- Bernal, J. L., Verde, L., & Riess, A. G. 2016, *J. Cosmology Astropart. Phys.*, 10, 019
- Betoule, M., Kessler, R., Guy, J., et al. 2014, *A&A*, 568, A22
- Beutler, F., Blake, C., Koda, J., et al. 2016, *MNRAS*, 455, 3230
- Beutler, F., Blake, C., Colless, M., et al. 2011, *MNRAS*, 416, 3017
- Blomqvist, M., Kirkby, D., Bautista, J. E., et al. 2015, *J. Cosmology Astropart. Phys.*, 11, 034
- Bonvin, V., Courbin, F., Suyu, S. H., et al. 2017, *MNRAS*, 465, 4914
- Brust, C., Cui, Y., & Sigurdson, K. 2017, *J. Cosmology Astropart. Phys.*, 8, 020
- Busca, N. G., Delubac, T., Rich, J., et al. 2013, *A&A*, 552, A96
- Calabrese, E., Hlozek, R. A., Battaglia, N., et al. 2013, *Phys. Rev. D*, 87, 103012
- Cardona, W., Kunz, M., & Pettorino, V. 2017, *J. Cosmology Astropart. Phys.*, 3, 056
- Carlstrom, J. E., Ade, P. A. R., Aird, K. A., et al. 2011, *PASP*, 123, 568
- Cole, S., Percival, W. J., Peacock, J. A., et al. 2005, *MNRAS*, 362, 505
- Cooke, R. J., Pettini, M., Jorgenson, R. A., Murphy, M. T., & Steidel, C. C. 2014, *ApJ*, 781, 31
- Cooke, R. J., Pettini, M., Nollett, K. M., & Jorgenson, R. 2016, *ApJ*, 830, 148
- Cuesta, A. J., Vargas-Magaña, M., Beutler, F., et al. 2016, *MNRAS*, 457, 1770
- Cybart, R. H., Fields, B. D., Olive, K. A., & Yeh, T.-H. 2016, *Reviews of Modern Physics*, 88, 015004
- Delubac, T., Bautista, J. E., Busca, N. G., et al. 2015, *A&A*, 574, A59
- Dhawan, S., Jha, S. W., & Leibundgut, B. 2017, ArXiv e-prints, arXiv:1707.00715
- du Mas des Bourboux, H., Le Goff, J.-M., Blomqvist, M., et al. 2017, ArXiv e-prints, arXiv:1708.02225
- Dunkley, J., Calabrese, E., Sievers, J., et al. 2013, *J. Cosmology Astropart. Phys.*, 7, 025
- Efstathiou, G. 2014, *MNRAS*, 440, 1138
- Eisenstein, D. J., & Hu, W. 1998, *ApJ*, 496, 605
- Eisenstein, D. J., Zehavi, I., Hogg, D. W., et al. 2005, *ApJ*, 633, 560
- Feeney, S. M., Mortlock, D. J., & Dalmasso, N. 2017, ArXiv e-prints, arXiv:1707.00007
- Fixsen, D. J. 2009, *ApJ*, 707, 916
- Fixsen, D. J., Cheng, E. S., Gales, J. M., et al. 1996, *ApJ*, 473, 576
- Follin, B., & Knox, L. 2017, ArXiv e-prints, arXiv:1707.01175
- Font-Ribera, A., Kirkby, D., Busca, N., et al. 2014, *J. Cosmology Astropart. Phys.*, 5, 027
- Freedman, W. L., Madore, B. F., Scowcroft, V., et al. 2012, *ApJ*, 758, 24
- Gelman, A., & Rubin, D. B. 1992, *Statist. Sci.*, 7, 457
- Heavens, A., Fantaye, Y., Sellentin, E., et al. 2017, ArXiv e-prints, arXiv:1704.03467
- Hildebrandt, H., Viola, M., Heymans, C., et al. 2017, *MNRAS*, 465, 1454
- Hinshaw, G., Larson, D., Komatsu, E., et al. 2013, *ApJS*, 208, 19
- Hong, T., Han, J. L., & Wen, Z. L. 2016, *ApJ*, 826, 154
- Hou, Z., Reichardt, C. L., Story, K. T., et al. 2014, *ApJ*, 782, 74
- Izotov, Y. I., Thuan, T. X., & Guseva, N. G. 2014, *MNRAS*, 445, 778
- Joudaki, S., Blake, C., Heymans, C., et al. 2017, *MNRAS*, 465, 2033

<sup>19</sup> <http://getdist.readthedocs.io/en/latest/>

- Kazin, E. A., Koda, J., Blake, C., et al. 2014, *MNRAS*, 441, 3524
- Köhlinger, F., Viola, M., Joachimi, B., et al. 2017, *MNRAS*, 471, 4412
- Lewis, A., & Bridle, S. 2002, *Phys. Rev. D*, 66, 103511
- Louis, T., Grace, E., Hasselfield, M., et al. 2017, *J. Cosmology Astropart. Phys.*, 6, 031
- Marcucci, L. E., Mangano, G., Kievsky, A., & Viviani, M. 2016, *Physical Review Letters*, 116, 102501
- Peimbert, A., Peimbert, M., & Luridiana, V. 2016, *Rev. Mexicana Astron. Astrofis.*, 52, 419
- Percival, W. J., Ross, A. J., Sánchez, A. G., et al. 2014, *MNRAS*, 439, 2531
- Pettini, M., & Cooke, R. 2012, *MNRAS*, 425, 2477
- Planck Collaboration, Ade, P. A. R., Aghanim, N., et al. 2016, *A&A*, 594, A13
- Planck Collaboration Int. LI. 2016, *ArXiv e-prints*, arXiv:1608.02487
- Planck Collaboration Int. XLVI. 2016, *A&A*, 596, A107
- Planck Collaboration XI. 2016, *A&A*, 594, A11
- Reid, B., Ho, S., Padmanabhan, N., et al. 2016, *MNRAS*, 455, 1553
- Riemer-Sørensen, S., Kotuš, S., Webb, J. K., et al. 2017, *MNRAS*, 468, 3239
- Riemer-Sørensen, S., & Sem Janssen, E. 2017, *ArXiv e-prints*, arXiv:1705.03653
- Riess, A. G., Macri, L., Casertano, S., et al. 2009, *ApJ*, 699, 539
- . 2011, *ApJ*, 730, 119
- Riess, A. G., Macri, L. M., Hoffmann, S. L., et al. 2016, *ApJ*, 826, 56
- Ross, A. J., Samushia, L., Howlett, C., et al. 2015, *MNRAS*, 449, 835
- Sherwin, B. D., van Engelen, A., Sehgal, N., et al. 2016, *ArXiv e-prints*, arXiv:1611.09753
- Sievers, J. L., Hlozek, R. A., Nolte, M. R., et al. 2013, *J. Cosmology Astropart. Phys.*, 10, 60
- Slosar, A., Iršič, V., Kirkby, D., et al. 2013, *J. Cosmology Astropart. Phys.*, 4, 026
- Story, K. T., Reichardt, C. L., Hou, Z., et al. 2013, *ApJ*, 779, 86
- Thornton, R. J., Ade, P. A. R., Aiola, S., et al. 2016, *ApJS*, 227, 21
- van Engelen, A., Keisler, R., Zahn, O., et al. 2012, *ApJ*, 756, 142
- Veropalumbo, A., Marulli, F., Moscardini, L., Moresco, M., & Cimatti, A. 2016, *MNRAS*, 458, 1909
- Wang, Y., Xu, L., & Zhao, G.-B. 2017, *ArXiv e-prints*, arXiv:1706.09149
- Weinberg, D. H., Mortonson, M. J., Eisenstein, D. J., et al. 2013, *Phys. Rep.*, 530, 87
- Zhang, B. R., Childress, M. J., Davis, T. M., et al. 2017, *MNRAS*, 471, 2254